Lanthanide cofactors accelerate DNA-catalyzed synthesis of branched RNA

Fatemeh Javadi-Zarnaghi and Claudia Höbartner*

Research Group Nucleic Acid Chemistry, Max Planck Institute for Biophysical Chemistry, Göttingen, Germany

General Information

Standard 5'-*O*-DMT-protected 3'-β-cyanoethyl phosphoramidites of N^6-benzoyl-2'-deoxyadenosine, N^4-acetyl-2'-deoxycytidine, N^2-(*N*,*N*-dimethylamino)methylene-2'-deoxyguanosine, and thymidine were from SAFC/Sigma-Aldrich. 5'-*O*-DMT-2'-*O*-TOM-protected 3'-β-cyanoethyl phosphoramidites of N^6-acetyladenosine, N^4-acetylcytidine, N^2-acetylguanosine, and uridine were from ChemGenes. Benzylthiotetrazole (BTT) was from Carbosynth (UK). Ribonucleotide triphosphates (NTPs) for in vitro transcription reactions were from Jena Bioscience, and α-^{32}P-dATP (3000 Ci/mmol) and γ-^{32}P-ATP (3000 Ci/mmol) was from Perkin Elmer. T4 RNA ligase, T4 polynucleotide kinase (PNK), and DNase I were from Fermentas, and Klenow fragment was from Jena Bioscience.

Table S1. Oligonucleotides used in this study

a. RNA substrates

1	*Acceptor*	5′-UAAUACG**A**CUCAC**UA**UA-3′
1i	*Inactive acceptor*	5′-UAAUACGACUCACU(**dA**)UA-3′
2	*Donor*	5′-pppGGAAGAGAUGGCGACGG-3′
2s	*Short donor*	5′-pppGGAAGAGAUGG-3′
2i	*Inactive donor*	5′- pGGAAGAGAUGGCGACGG-3′
2a	*Alternative donor*	5′-pppGAAUAACAUCCACACCA-3′

Branch-site nucleotides in **1** are marked in bold letters (A8 for 7S11, U14 for 9F13 and A15 for 9F7).

b. Deoxyribozymes

9F7 for **2**	5′-CAACGTCGCCATCTC**AATGAGGCTTGGCAGGGATTTAGTATTTTAACACTCCCGG**GTAGTCGTATTA-3′
9F7 for **2s**	5′-CAACATCTC**AATGAGGCTTGGCAGGGATTTAGTATTTTAACACTCCCGG**GTAGTCGTATTA-3′
9F7min for **2a**	5′-TGGTGTGGATGTT**AATGAGGCTTGGCAGGGACTCCCGG**GTAGTCGTATTA-3′
9F7min for **2**	5′-CAACGTCGCCATCTC**AATGAGGCTTGGCAGGGACTCCCGG**GTAGTCGTATTA-3′
9F7min-1 for **2**	5′-CAACGTCGCCATCTC**AATGAGGCTTGGCAGGGCTCCCGG**GTAGTCGTATTA-3′
9F7min-2 for **2**	5′-CAACGTCGCCATCTC**AATGAGGCTTGGCAGGGTCCCGG**GTAGTCGTATTA-3′
9F7min-3 for **2**	5′-CAACGTCGCCATCTC**AATGAGGCTTGGCAGGGCCCGG**GTAGTCGTATTA-3′
9F13 for **2**	5′-CAACGTCGCCATCTC**AGGATGTGGGGTTTTGCCCGAGGGTATGGCAGTGGGGA**GAGAGTCGTATTA-3′
9F13 for **2s**	5′-CAACATCTC**AGGATGTGGGGTTTTGCCCGAGGGTATGGCAGTGGGGA**GAGAGTCGTATTA-3′
9F13min for **2**	5′-CAACGTCGCCATCTC**AGGATGTGGGGTGCCCTTGGGGA**GAGAGTCGTATTA-3′
9F13min for **2s**	5′-CGCCATCTC**AGGATGTGGGGTGCCCTTGGGGA**GAGAGTCGTATTA-3′
7S11 for **2**	5′-CCGTCGCCATCTC**CAGTGCAGGGC**GTGAG**GGCTCGG**TTCCCGTATTATCC-3′

The bold nucleotides represent the catalytic loop regions. The non-bold nucleotides constitute the binding arm for the RNA substrates. The underlined nucleotides in 7S11 form a paired region with the donor RNA in the 3HJ structure.

c. Templates and promoter strand for in vitro transcription of donor strands

template for **2**	5′-CCGTCGCCATCTCTTCCTATAGTGAGTCGTATTACAG-3′
template for **2a**	5′-TGGTGTGGATGTTATTCTATAGTGAGTCGTATTACAG-3′
template for **2s**	5′-CCATCTCTTCCTATAGTGAGTCGTATTACAG-3′
T7 promoter	5′-CTGTAATACGACTCACTATA-3′

d. Template DNA for 3'-^{32}P-labeling of deoxyribozyme libraries

T-9F7	5′-GTTAATACGACTACCC-3′
T-9F13	5′-GTTAATACGACTCTCTC-3′

e. complementary DNA for HPLC analysis of Tb^{3+} effect on triphosphorylated donor

Complement for **2**	5′-CCGTCGCCATCTCTTCC-3′

Unmodified DNA oligonucleotides were purchased from Sigma Aldrich and purified by denaturing PAGE (20% or 15% polyacrylamide). The RNA donor strands were prepared by in vitro transcription using T7 RNA polymerase and synthetic DNA templates. The RNA acceptor substrates and CoMA pools were prepared by solid-phase synthesis, following our previously described procedures.[1]

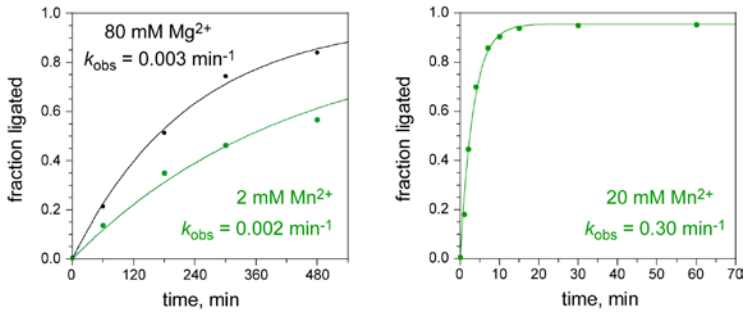

Figure S1. Ligation kinetics of 9F7-catalyzed ligation of acceptor RNA **1** and donor RNA **2** in 50 mM HEPES buffer pH 7.5, 150 mM NaCl, 2 mM KCl, 37°C, and the indicated concentration of Mg^{2+} or Mn^{2+}.

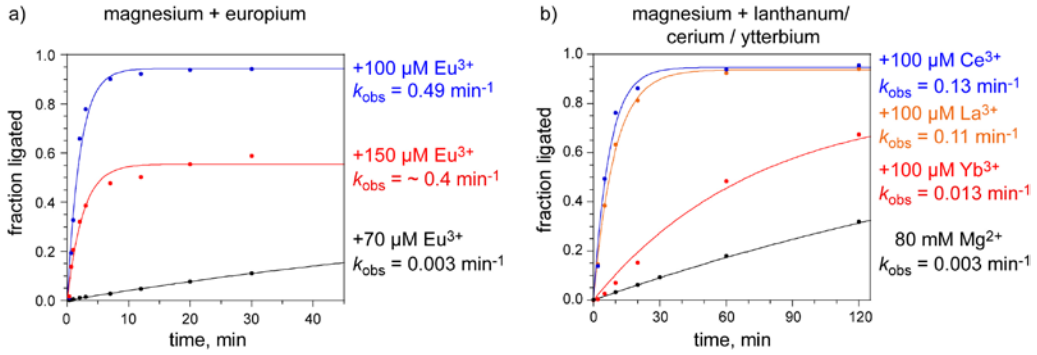

Figure S2. a) Ligation kinetics of 9F7-catalyzed ligation with magnesium and europium; compare **Figure 1c,d** for comparable data with Tb^{3+} and Gd^{3+}. b) Ligation kinetics of 9F7-catalyzed ligation with magnesium and lanthanum, cerium and ytterbium. The data for ligation in absence of lanthanides (only 80 mM Mg^{2+}) is plotted for comparison.

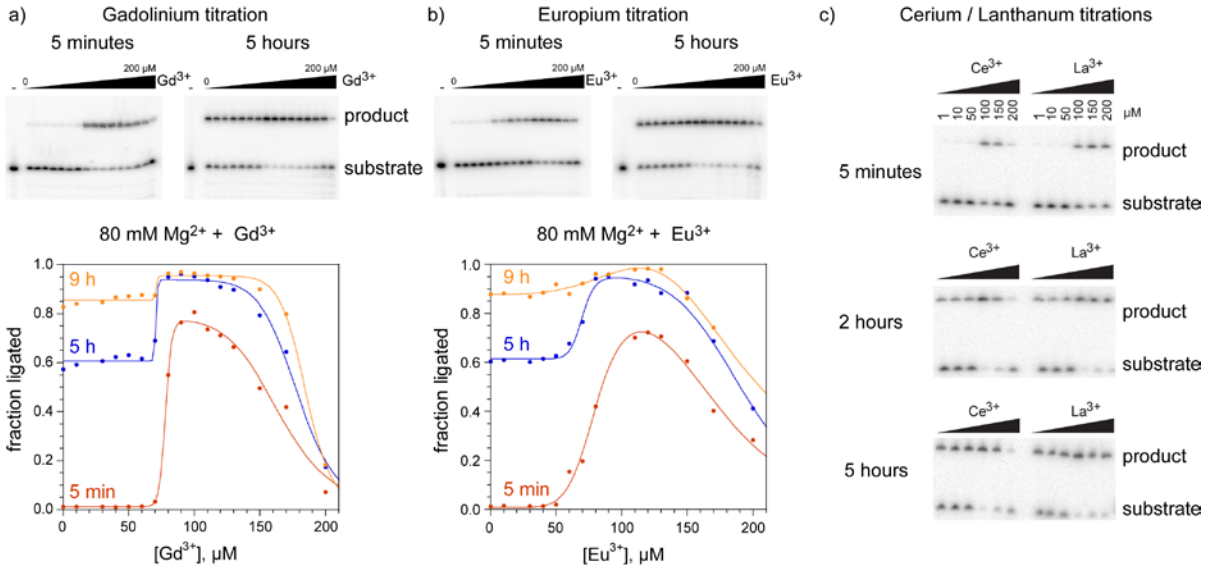

Figure S3. Dependence of ligation yield on concentration of a) Gd^{3+}, b) Eu^{3+}, c) La^{3+} and Ce^{3+}, in presence of 80 mM Mg^{2+}, at pH 7.5, 37°C. Yields are determined by quantification of ^{32}P-images after gel electrophoresis. Fits are to the equation: fraction ligated = $\{Y_0+Y_a \bullet [Ln^{3+}]^n/([Ln^{3+}]_{1/2,a}{}^n + [Ln^{3+}]^n)\} \bullet \{1-[Ln^{3+}]^m/([Ln^{3+}]_{1/2,b}{}^m + [Tb^{3+}]^m)\}$. Fit values are summarized in Table S2. Compare **Figure 2** (in manuscript) for comparable data with terbium. The fit equation describes a model with independent binding sites for lanthanide ions that activate or inhibit the deoxyribozyme. A similar model with n activating and m inhibitory lanthanide ions was used by Silverman and coworkers to describe the lanthanide dependent activity of DNA-catalyzing deoxyribozymes.[4] Here, the model is expanded to additionally address the "background" activity of 9F7 with divalent metal ions (Y_0).

Table S2. Fit values for Figure 2 and S3.

Titration	reaction time	Y_0	Y_a	$[Ln^{3+}]_{1/2,a}$ µM	n	$[Ln^{3+}]_{1/2,b}$ µM	m
Tb^{3+} with 80 mM Mg^{2+}	5 min	0.02	0.91	71	18	139	5
	5 h	0.66	0.31	67	60	162	5
Tb^{3+} with 20 mM Mn^{2+}	1 min	-	0.9	4.6	1.3	50	1.8
	60 min	-	0.95	-	-	97	2.2
Gd^{3+} with 80 mM Mg^{2+}	5 min	0.01	0.76	77	32	164	8
	5 h	0.60	0.33	70	118	178	11
Eu^{3+} with 80 mM Mg^{2+}	5 min	0.008	0.76	81	7	171	5
	5 h	0.61	0.33	69	14	192	7

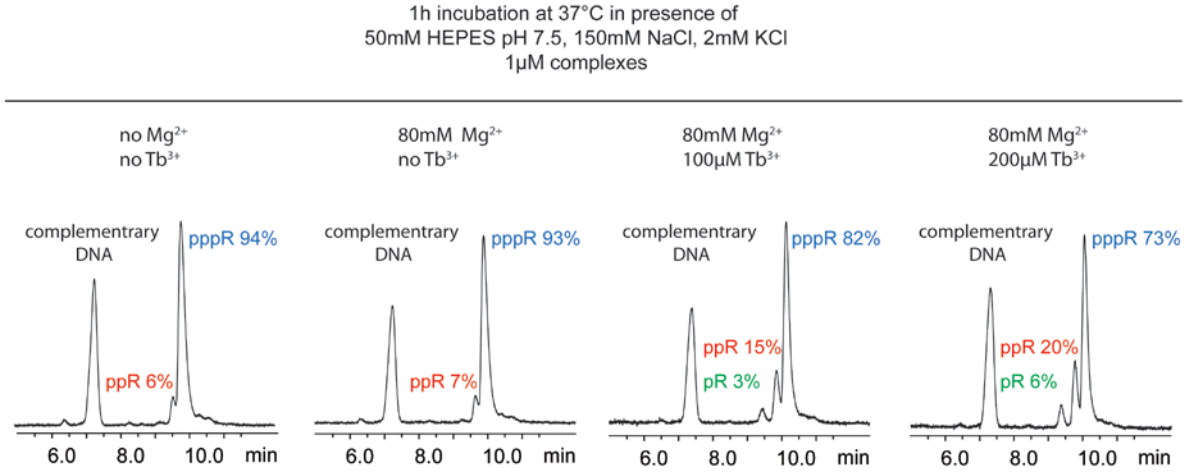

Figure S4. HPLC analysis of the fate of triphosphate donor RNA in presence of Tb^{3+}. RNA **2** (labeled pppR) was hybridized to its complementary DNA to resemble the deoxyribozyme binding arm. Anion exchange HPLC on Dionex-DNAPac PA200, 80°C. Quantification via area integration of UV^{260} trace. ppR is the diphosphorylated analog of RNA **2**, and pR is the 5'-monophosphorylated analog of RNA **2**. Identification was performed via MS and coinjection with authentic samples.

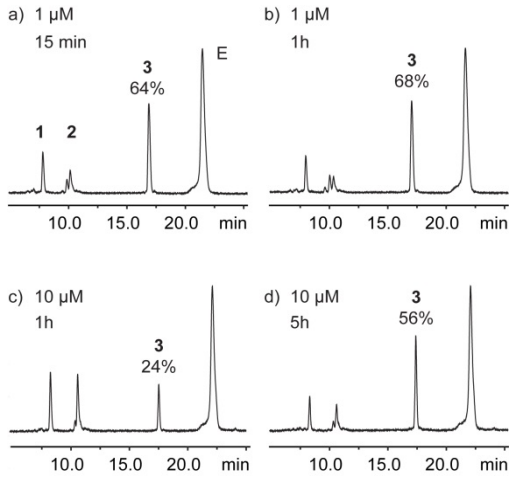

Figure S5. HPLC analysis of preparative ligation reactions. Conditions: donor (**1**) : acceptor (**2**) : deoxyriboyzme (E) = 1 : 1 : 1; 80 mM Mg^{2+}, 100 µM Tb^{3+}, 37°C. Concentration of pre-ligation complex and incubation time as indicated for each panel. Anion exchange HPLC on Dionex-DNAPac PA200, 80°C. Quantification via area integration of UV^{260} trace.

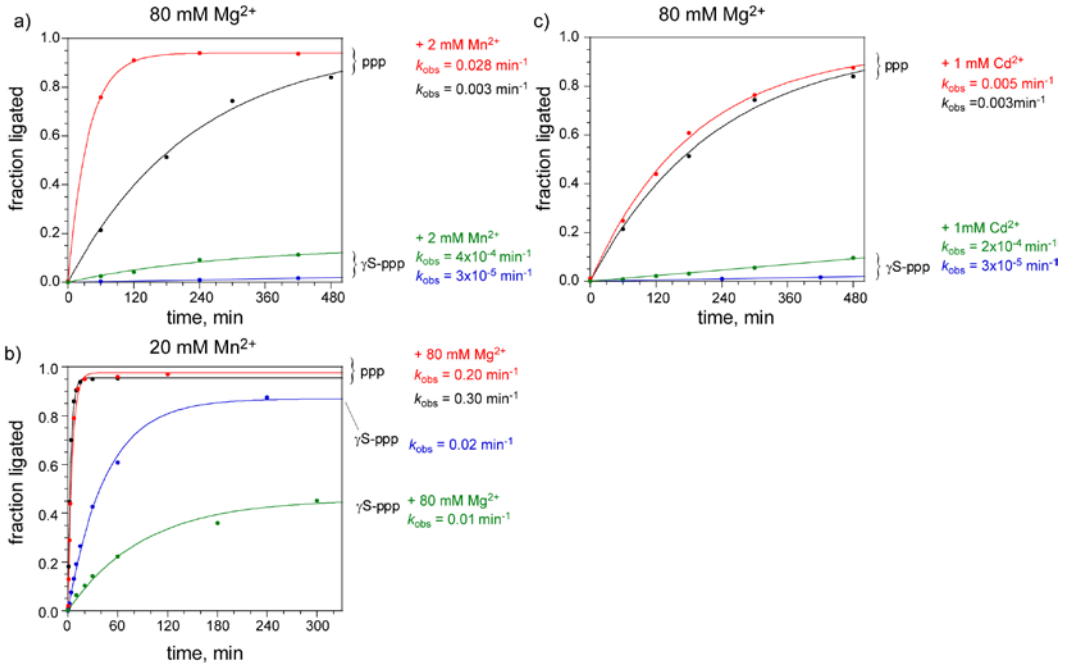

Figure S6. Phosphorothioate effects and metal ion rescue attempts for 9F7-catalyzed ligation of RNAs **1** and **2** with gamma phosphorothioate. See manuscript text for details.

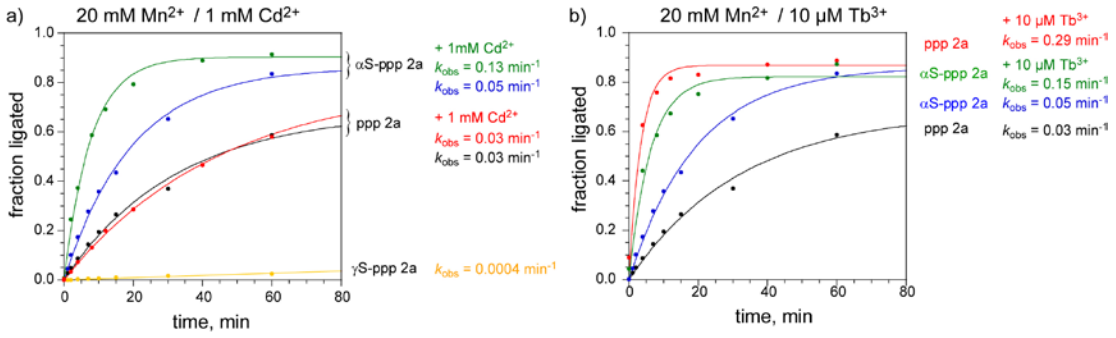

Figure S7. Phosphorothioate effects and metal ion rescue attempts for 9F7-catalyzed ligation of RNAs **1** and alternative donor **2a** (containing only one single G on 5' end) with alpha and gamma phosphorothioate. Comparison of Cd^{2+} and Tb^{3+} effect on ligation of PO and PS donor substrate in presence of 20 mM Mn^{2+}. The alternative substrate **2a** is ligated 10-fold more slowly than original substrate **2**. 1 mM Cd^{2+} and 10 µM Tb^{3+} have comparable 3-fold effect for acceleration of alpha PS. In contrast, the ligation of PO substrate **2a** is not affected by 1 mM Cd^{2+} but 10-fold accelerated by 10 µM Tb^{3+}.

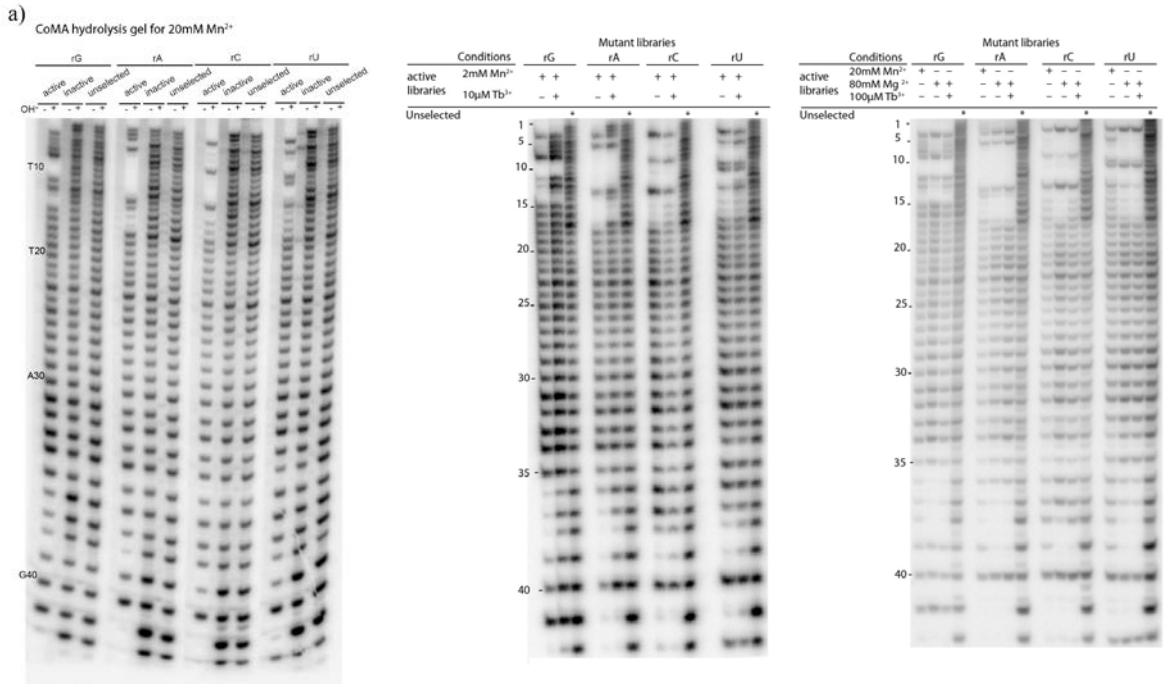

Figure S8 continued on next page

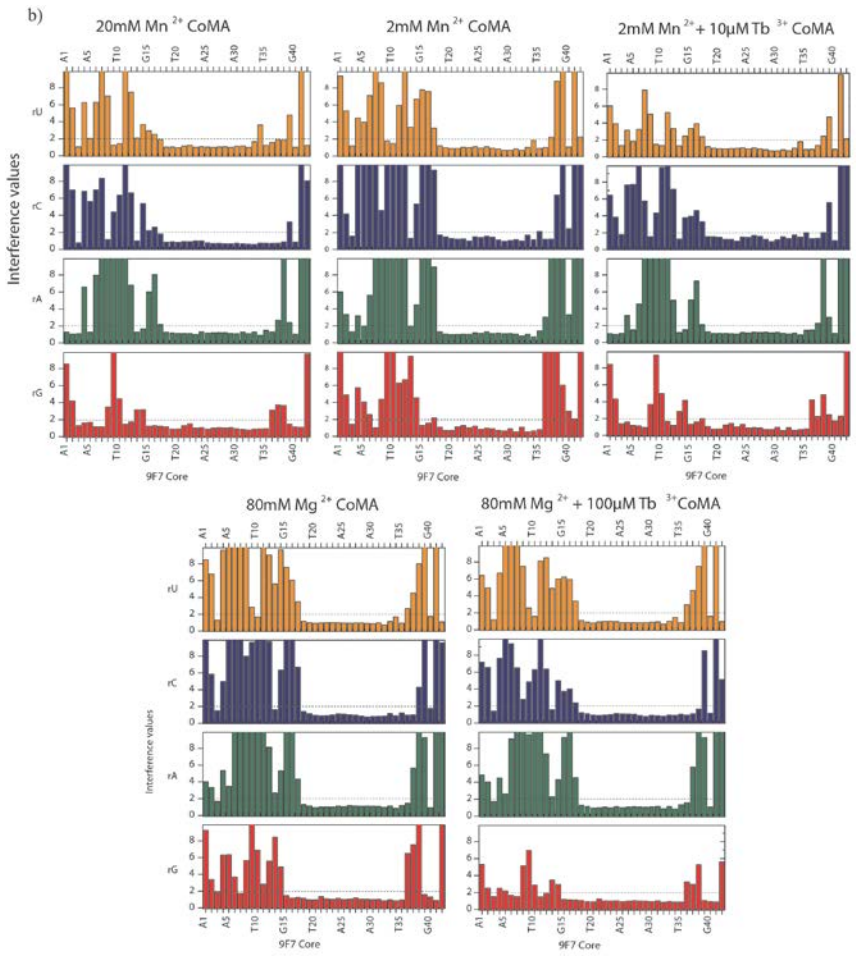

Figure S8. Full hydrolysis gels (a) and interference values (b) for 9F7 CoMA. a) left: The full CoMA hydrolysis gel for separation after ligation with 20 mM Mn^{2+}. Middle and right: The hydrolysis pattern of active and unselected libraries for the 5 conditions applied in this study. For each mutant library, the active and inactive portions, as well as the unselected library were subjected to hydrolysis and the products were resolved on denaturing sequencing gel. In all cases, hydrolysis was performed with 10 mM freshly made NaOH by heating at 95°C for 10 min. (A water control was done for each hydrolysis sample and was run aside the sample shown in the left gel, labeled "–"). b) The interference value for each library at indicated conditions was calculated from volume analysis of PhosphorImages. Interference value = (intensity in unseparated library) / (intensity in active fraction).

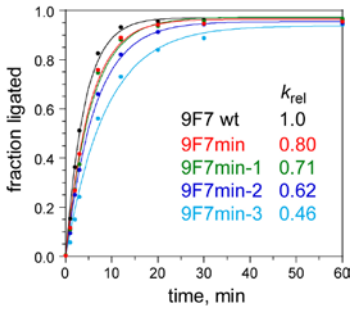

Figure S9. Kinetic data for shortened variants of 9F7 (based on CoMA results) at 20 mM Mn^{2+}, 37°C. k_{rel} was defined with the ratio of k_{obs} for shortened variants over k_{obs} for 9F7 wt.

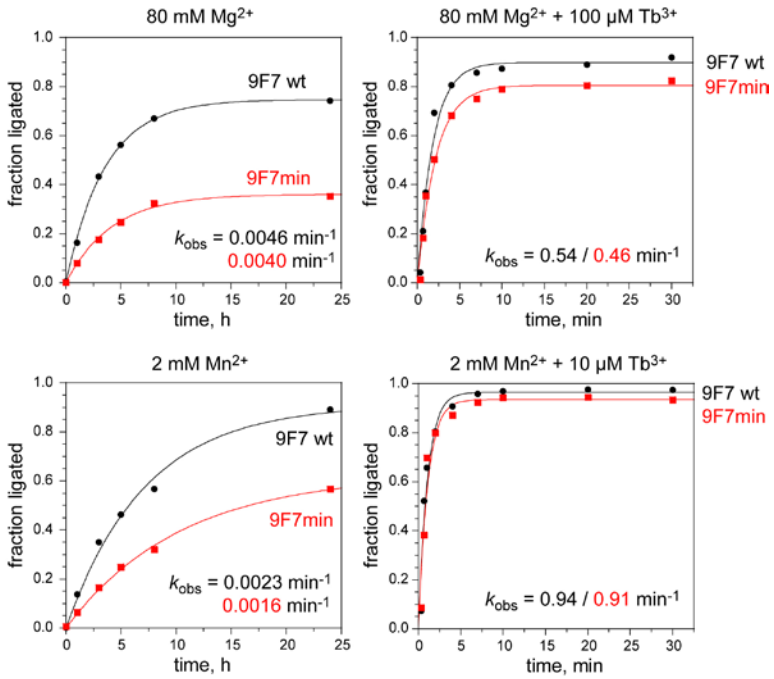

Figure S10. Kinetic data for 9F7wt and 9F7min, including Tb^{3+} acceleration with Mn^{2+} and Mg^{2+} (bottom right is same as in **Figure 5**; here reproduced for comparison)

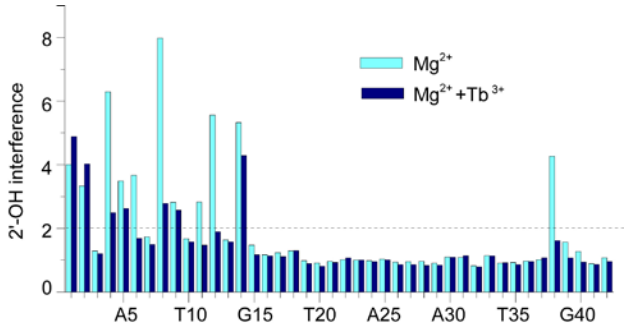

Figure S11. Rescue of 2'-OH effect by 100 µM Tb^{3+} in presence of 80 mM Mg^{2+}. Compare **Figure 6** for data with Mn^{2+} / Mn^{2+}+Tb^{3+}.

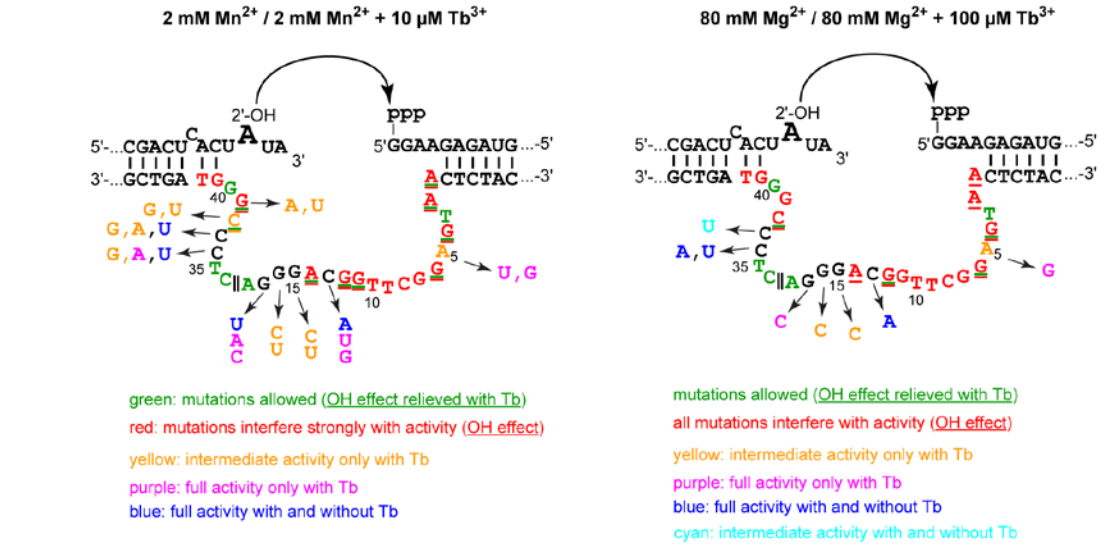

Figure S12. Graphical representation of CoMA results for the 9F7 deoxyribozyme, comparing mutation tolerance in absence and presence of Tb^{3+} (left: with 2 mM Mn^{2+}, right: with 80 mM Mg^{2+}). The color code is explained in the figure. The double line between A18 and C34 indicates the position of dispensable nucleotides that tolerated all mutations under all conditions.

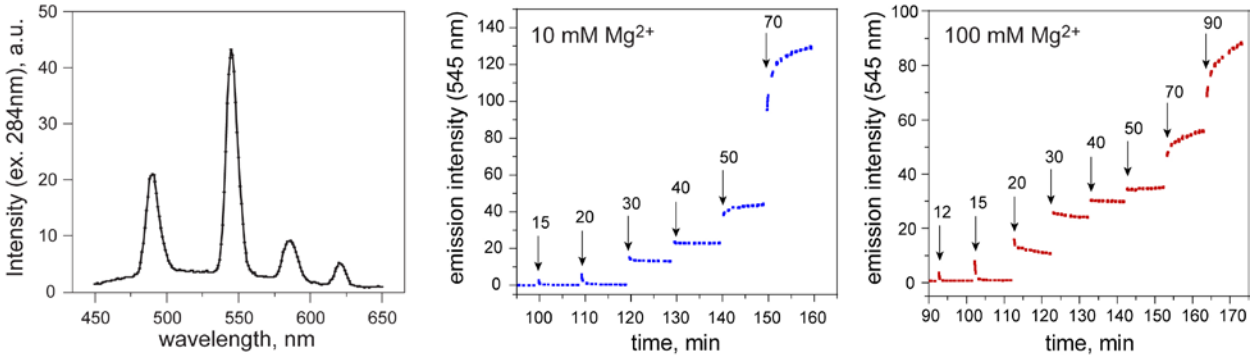

Figure S13. Left: Luminescence spectrum of Tb^{3+} bound to DNA (excitation at 284 nm). Middle & right: Time course of luminescence response upon Tb^{3+} titration in presence of 10 or 100 mM Mg^{2+}. These plots show excerpts for the data presented in Figure 7a, highlighting the three different modes of binding kinetics (< 20 µM, 20-50 µM, > 60µM) and demonstrating the importance of minimally 10 min equilibration time before taking the intensity reading. The arrows point at aliquot additions to reach the stated concentration (µM). Data acquisition started 10s after each aliquot addition.

Table S3. Fit values for Figure 7a,b.

divalent metal ion		I_{max}	$[Tb^{3+}]_{1/2}$ (µM)	n
Mn^{2+}	1 mM	245	69	2.4
	2 mM	167	67	2.6
	5 mM	145	86	2.8
	10 mM	82	101	2.7
Mg^{2+}	1 mM	508	93	2.9
	10 mM	493	100	2.8
	20 mM	436	114	2.6
	100 mM	373	139	2.6

Data were fit to the equation: $I = I_{max} \cdot [Tb^{3+}]^n / ([Tb^{3+}]_{1/2}{}^n + [Tb^{3+}]^n)$.

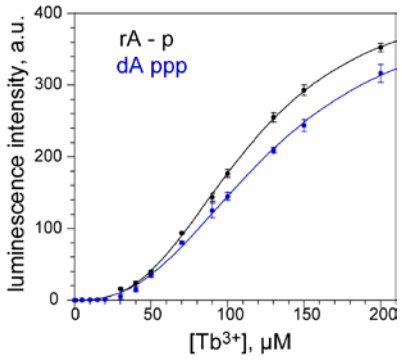

Figure S14. Tb^{3+} luminescence experiments with two inactive complexes, to check for differences in luminescence response when triphosphate on the donor or 2'-OH at the branch-site is absent. (black: with **1** and **2i**; blue: with **1i** and **2**.

Table S4. Summary of ligation yields of G4 mutants of 9F7min.

	nucleotide at position 4				
	G	A	C	U	
20 mM Mn^{2+}	0.88	0.12	0	0	% in 1 h
	0.95	**0.66**	0	0	% in 24 h
2 mM Mn^{2+} + 10 µM Tb^{3+}	0.91	0.23	0	0	
	0.95	**0.75**	0	0	
80 mM Mg^{2+}	0.23	0	0	0	
	0.78	0	0	0	
80 mM Mg^{2+} + 100 µM Tb^{3+}	0.88	0	0	0	
	0.91	0	0	0	

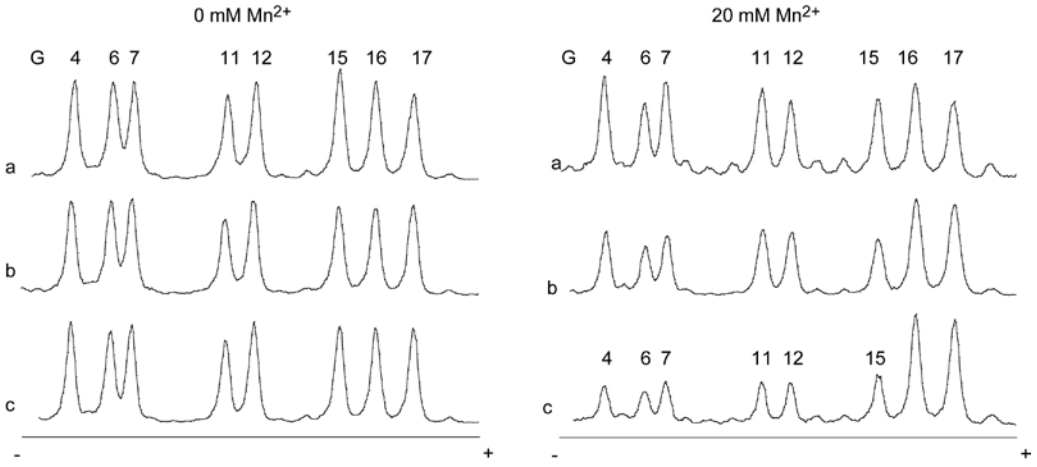

Figure S15. Line graph analysis of DMS probing data (compare Figure 8). In the absence of Mn^{2+} (left) all guanosines are equally accessible to DMS in all three complexes. The reduced intensity of G4-G15 with respect to G16 and G17 in the folded complex **c** in the presence of Mn^{2+} (right) is clearly visible. In complex **b**, the protection is still visible but less pronounced. (- and + indicate electrophoresis direction)

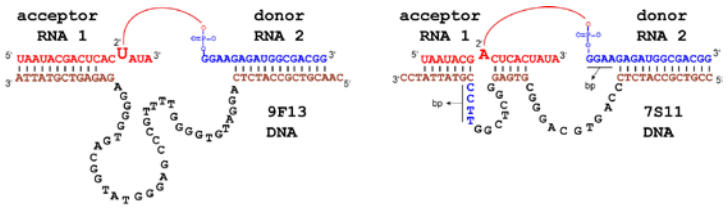

Figure S16. Comparison of sequences and branch-site context for 9F13[2] and 7S11[3]. bp = base-paired regions responsible for formation of 3-helix junction structure in 7S11.

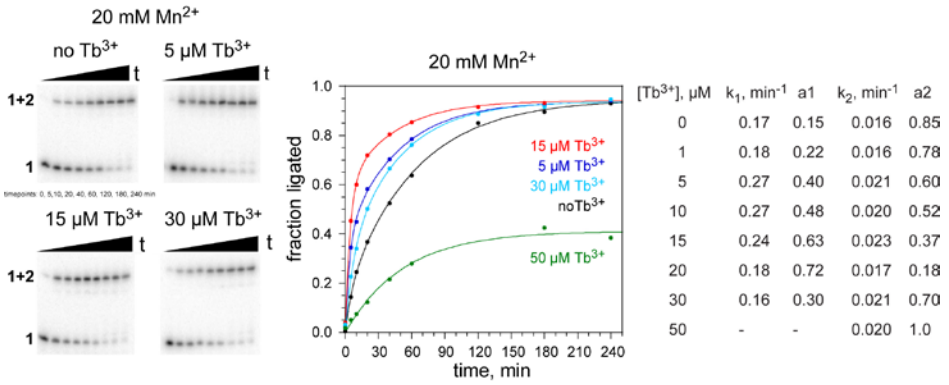

[Tb3+], μM	k1, min-1	a1	k2, min-1	a2
0	0.17	0.15	0.016	0.85
1	0.18	0.22	0.016	0.78
5	0.27	0.40	0.021	0.60
10	0.27	0.48	0.020	0.52
15	0.24	0.63	0.023	0.37
20	0.18	0.72	0.017	0.18
30	0.16	0.30	0.021	0.70
50	-	-	0.020	1.0

Figure S17. Kinetic analysis of 9F13-catalyzed RNA ligation with 20 mM Mn^{2+} and effect of Tb^{3+}. Fraction ligated vs. time data were fit to the equation fraction ligated = $Y_{max} \cdot [a1 \cdot (1–e^{-k_1 \cdot t}) + (1–a1) \cdot (1\text{-}e^{-k_2 \cdot t})]$. [Table: a2 = 1-a1].

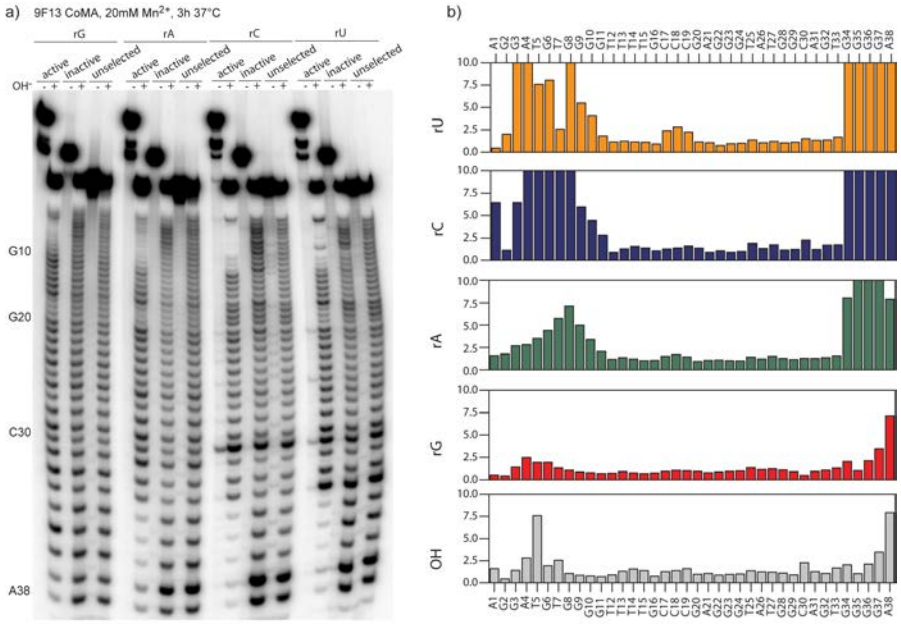

Figure S18. CoMA results for 9F13. a) hydrolysis gel after separation of active and inactive library fraction, ligation with 20 mM Mn^{2+} at 37°C. b) Interference values for all four libraries. The OH effect is plotted separately as the bottom graph (only at T5 and A38 severe inhibition was found in the presence of the 2'-OH tag), all other positions can be analyzed for the mutation effect.

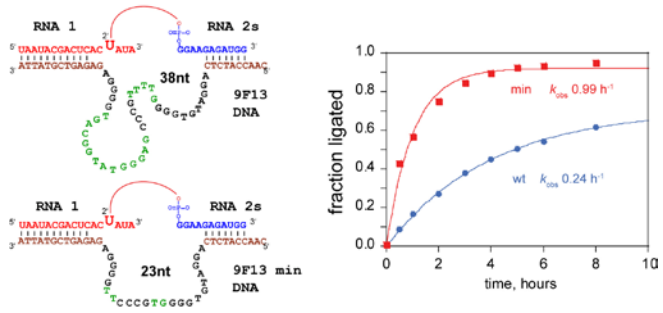

Figure S19. Schematic of 9F13 deoxyriboyzme. Nucleotides marked green in the full length wt sequence tolerate all mutations and are dispensable for activity. The minimized version 9F13min retains two green nucleotides between essential sections to maintain proper folding into an active conformation. Kinetic analysis shows 4-fold improved reaction kinetics for 9F13min. Ligation at pH 7.5, 37°C with 20 mM Mn^{2+} (note the slower reaction compared to data shown for 9F13wt in Fig S15 is due to the shorter binding arm of the donor substrate **2s** used).

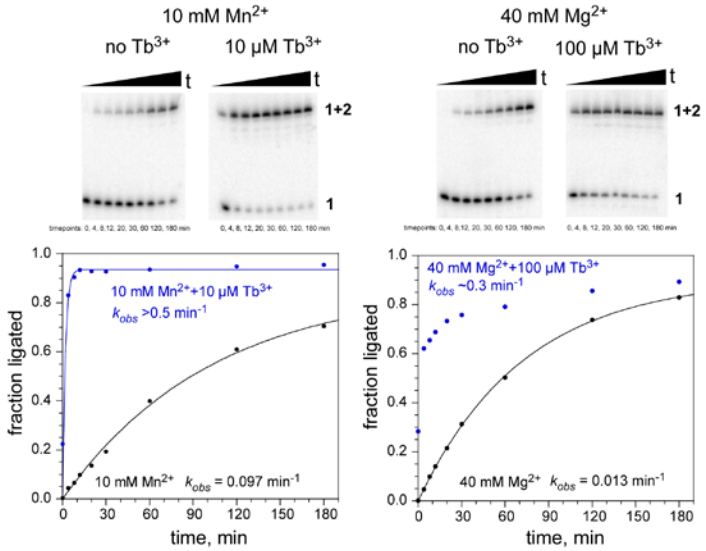

Figure S20. Kinetics of 7S11-catalyzed ligation of RNAs **1** and **2** at pH 7.5, 37°C using Mn^{2+} or Mg^{2+} as cofactor. Shown are gel images and kinetic curves for optimal Tb^{3+} concentrations in comparison to absence of Tb^{3+}. The available data in the presence of Tb^{3+} do not allow accurate determination of k_{obs} (estimates given in the Figure). The acceleration effect of Tb^{3+} is therefore ~20-fold with Mg^{2+}, and ~50-fold with Mn^{2+}.

Table S5. Tb^{3+}-stock solutions used for luminescence titrations. At every titration step, 1µL of the respective stock solution was added (sample volume at start of the experiment 600 µL).

					Preparation of individual stock conc.		
No	Final Tb^{3+} concentration (µM)	Individual stock conc. for each titration step (µM)	Sample volume after each addition (µL)	Dilution factor	Parent Tb^{3+} stock (mM)	Volume of parent stock soln. (µL)	H_2O (µL)
1	1.0	601	601	1.002	10	30.0	470.0
2	1.5	302	602	1.003	10	15.1	484.9
3	2.0	303	603	1.005	10	15.2	484.8
4	3.0	606	604	1.007	10	30.3	469.7
5	4.0	608	605	1.008	10	30.4	469.6
6	5.0	610	606	1.010	10	30.5	469.5
7	7.0	1219	607	1.012	10	61.0	439.0
8	10	1831	608	1.013	10	91.6	408.4
9	12	1228	609	1.015	10	61.4	438.6
10	15	1842	610	1.017	10	92.1	407.9
11	20	3070	611	1.018	100	15.4	484.6
12	30	6140	612	1.020	100	30.7	469.3
13	40	6160	613	1.022	100	30.8	469.2
14	50	6180	614	1.023	100	30.9	469.1
15	70	12350	615	1.025	100	61.8	438.2
16	90	12390	616	1.027	100	62.0	438.0
17	100	6260	617	1.028	100	31.3	468.7
18	130	18640	618	1.030	100	93.2	406.8
19	150	12510	619	1.032	100	62.6	437.4
20	200	31150	620	1.033	100	155.8	344.2

References for supporting information

[1] F. Wachowius, F. Javadi-Zarnaghi, C. Höbartner, *Angew. Chem. Int. Ed.* **2010**, *49*, 8504-8508.
[2] Y. Wang, S. K. Silverman, *J. Am. Chem. Soc.* **2003**, *125*, 6880-6881.
[3] R. L. Coppins, S. K. Silverman, *J. Am. Chem. Soc.* **2005**, *127*, 2900-2907.
[4] V. Dokukin, S.K. Silverman, *Chem. Sci.* **2012**, *3*, 1707-1714.